Journal of Power Sources 196 (2011) 6138–6143

Contents lists available at ScienceDirect

Journal of Power Sources

journal homepage: www.elsevier.com/locate/jpowsour

Anodic oxidation of ethanol on core-shell structured Ru@PtPd/C catalyst in alkaline media

Haili Gao[a,b], Shijun Liao[a,b,*], Zhenxing Liang[a,b], Huagen Liang[a,b], Fan Luo[a,b]

[a] School of Chemistry and Chemical Engineering, South China University of Technology, Guangzhou 510641, China
[b] Key Lab for Fuel Cell Technology of Guangdong Province & Key Lab of Enhanced Heat Transfer and Energy Conservation, Ministry of Education, China

ARTICLE INFO

Article history:
Received 14 January 2011
Received in revised form 14 March 2011
Accepted 15 March 2011
Available online 23 March 2011

Keywords:
Ethanol electrooxidation
Electrocatalysts
Fuel cell
Alkaline media

ABSTRACT

The direct ethanol fuel cell has been attracting increased attention due to its safety and the wider availability of ethanol as compared with methanol. The present work investigates the anodic oxidation of ethanol on a core-shell structured Ru@PtPd/C catalyst in alkaline media. The catalyst shows high activity toward the anodic oxidation of ethanol; with 18 wt.% ruthenium as the core and 12 wt.% PtPd (Pt:Pd = 1:0.2) as the active shell, its activity in terms of PtPd loading is 1.3, 3, 1.4, and 2.0 times as high as that of PtPd/C, PtRu/C, Pd/C, and Pt/C, respectively, indicating high utilization of Pt and Pd. The ratio of forward peak current density to backward peak current density (I_f/I_b) reaches 1.5, which is 1.9 times that of PtPd/C catalyst, revealing high poisoning tolerance to the intermediates in ethanol electrooxidation. In addition, the stability of Ru@PtPd/C is higher than that of Pt/C and PtPd/C, as evidenced by chronoamperometric evaluations. The catalyst is extensively characterized by transmission electron microscopy (TEM), X-ray diffraction (XRD), and X-ray photoelectron spectroscopy. The core-shell structure of the catalyst is revealed by XRD and TEM.

1. Introduction

In the last two decades, the direct methanol fuel cell (DMFC) has been considered an ideal mobile fuel cell system for portable electronics and transportation applications because of its simple construction, high weight-volume energy densities, low operation temperatures, convenient fuel feeding, and other features [1]. However, DMFC commercialization is hampered by some serious problems, including crossover of methanol through the membrane [2,3] – leading to a mixed potential in the oxygen reduction reaction that decreases energy efficiency – and methanol's toxicity, which damages the human optic nerve and the environment [4].

Other small-molecule alcohols (e.g. ethanol, ethylene glycol) have thus emerged as potential alternative fuels. In particular, the direct ethanol fuel cell (DEFC) has been the topic of numerous research papers [5–8], as ethanol is non-toxic, inexpensive, has a higher theoretical mass energy than methanol (8 kWh kg^{-1} vs. 6.1 kWh kg^{-1}) [9], and is considered a "green" chemical because it can be produced in large quantities as a renewable biofuel from the fermentation of biomass [8], leaving the natural balance of carbon dioxide in the atmosphere unchanged, in contrast to the effects of fossil fuels [10].

Platinum is at present the best-known catalyst for the adsorption and dissociation of small organic molecules [11]. Most studies of ethanol electrooxidation have focused on using platinum in an acidic electrolyte [12–14]. The electrooxidation of ethanol is reported to proceed via a dual pathway mechanism [15]: ethanol is oxidized to acetaldehyde and subsequently to acetic acid, transferring only four electrons in the process; alternatively, the carbon–carbon bond can be cleaved in ethanol or acetaldehyde, yielding the adsorbed single carbon species CO_{ad} [16] and $CH_{x,ad}$ (with $x = 1$ in acidic media) [13]. These species can subsequently be oxidized to CO_2, liberating 12 electrons in total. Surface adsorbed CO is still identified as the leading intermediate in ethanol electrooxidation, as it is in methanol electrooxidation [17]. The desired reaction in DEFCs is the complete electrooxidation of ethanol to CO_2 and water, involving the transfer of 12 electrons per ethanol molecule. However, catalysts that can cleave the C–C bond in ethanol and have the capacity for complete ethanol electrooxidation have not been realized [18]. Consequently, much current effort is being focused on reducing the amounts of adsorbed intermediates. PtRu catalyst, which has proven the best anode electrocatalyst in DMFCs, has been widely investigated in DEFCs [19–21]. Ruthenium's promoting effect begins at a concentration of at least 20% [11]. Unfortunately, the high price of platinum coupled with high

* Corresponding author at: School of Chemistry and Chemical Engineering, South China University of Technology, Guangzhou 510641, China. Tel.: +86 20 8711 3586; fax: +86 20 8711 3586.
E-mail address: chsjliao@scut.edu.cn (S. Liao).

0378-7753/$ – see front matter © 2011 Elsevier B.V. All rights reserved.
doi:10.1016/j.jpowsour.2011.03.031

Pt loading remains a bottleneck in the further development of DEFCs.

Core-shell nanostructures are emerging as effective ways to increase the utilization efficiency of precious metal electrocatalysts, since the precious metal can be highly dispersed on a core formed of relative inexpensive metals. Because these structures have relatively lower densities and higher surface areas than their solid counterparts, they not only achieve high catalytic performance and precious metal utilization efficiency but also reduce catalyst cost [22].

In our previous work [23], a low platinum content Ru@Pt/C catalyst with a relatively inexpensive ruthenium core was prepared by a two-stage procedure, and its performance in acidic media was investigated. In the present work we use a platinum–palladium alloy as the shell rather than just platinum, preparing a Ru@PtPd/C catalyst that exhibits much higher activity toward the anodic oxidation of ethanol in alkaline media than do Pd/C, PtPd/C, or PtRu/C.

2. Experimental

2.1. Catalyst preparation

Ru@PtPd/C catalyst (30 wt.% total metal load) with PtPd on the surface layer of a Ru core was synthesized via a facile, two-stage procedure.

Ru/C: To prepare Ru/C catalyst, Vulcan XC-72 carbon (Cabot Corp.) pretreated with 10% HNO_3 and 30% H_2O_2 was used as the carbon support. 103.5 mg ruthenium chloride was dissolved in 2 ml diluted HCl solution, followed by the addition of 155 mg pretreated carbon powder. The suspension was stirred to facilitate impregnation, and then heated in a water bath at 70 °C to evaporate the solvents, followed by drying in an oven and grinding. Finally, Ru/C was prepared by reducing the sample in a tubular furnace at 200 °C for 2 h under a hydrogen flow.

Ru@PtPd/C: 4.2 mg palladium chloride ($PdCl_2$) was dissolved in concentrated HCl in a flask, followed by the addition of 15 ml chloroplatinic acid/ethylene glycol (EG) solution, containing 60.3 mg chloroplatinic acid. 103.1 mg sodium citrate was added to the flask as a complexing agent and stirred for 1 h to entirely dissolve the sodium citrate. Afterwards, the as-prepared Ru/C was added to the mixture, followed by pH adjustment to >10 by the drop-wise addition with vigorous stirring of a 5 wt.% KOH/EG solution. The mixture was then transferred into a Teflon-lined autoclave and conditioned at 120 °C for 6 h, followed by filtering, washing, and vacuum drying at 70 °C. Ru@PtPd/C catalyst with a nominal atomic ratio of Ru:Pt:Pd = 1:0.3:0.06 was obtained. A Ru@Pt/C catalyst (mole ratio Ru:Pt = 1:0.3) was prepared using the same procedures but omitting the $PdCl_2$.

For comparison, 12 wt.% PtPd/C (mole ratio Pt:Pd = 1:0.2), 20 wt.% Pd/C, and 30 wt.% PtRu/C (mole ratio Pt:Ru = 1:1) were prepared using the same organic colloidal approach.

2.2. Characterization

X-ray powder diffraction (XRD) was carried out on a Shimadzu XD-3A (Japan) using filtered Cu Kα radiation, operated at 40 kV and 40 mA. The 2θ angular region between 20° and 80° was explored at a scan rate of 4° min^{-1}. The morphology, particle size, and particle size distribution of the catalysts were observed using transmission electron microscopy (TEM; JEOL JEM-2010HR, Japan) operated at 200 kV. Specimens for TEM examination were prepared by placing a drop of Ru@PtPd/C catalyst dispersion in ethanol onto a carbon-coated copper grid, followed by natural evaporation of the solvent at room temperature. X-ray photoelectron spectroscopy (XPS) measurement was carried out in an ultrahigh vacuum on a PerkinElmer PHI1600 system (PerkinElmer, USA) using a single Mg Kα X-ray source operating at 300 W and 15 kV of voltage. The Pt 4f, Ru 3p, and Pd 3d signals were collected and analyzed by deconvolution of the spectra using XPS Peak software. The binding energies were calibrated using the C 1s peak of graphite at 284.5 eV as a reference.

2.3. Electrochemical measurements

The prepared catalysts' electrocatalytic activities for ethanol electrooxidation were investigated in a nitrogen-saturated solution of 1.0 M KOH + 1.0 M ethanol using a three-electrode electrochemical cell. The counter and reference electrodes were a platinum wire and a Hg/HgO (1.0 M KOH solution) electrode, respectively. The working electrode was a thin film of Nafion-impregnated catalyst cast on a glassy carbon electrode (5 mm in diameter). 5 mg of catalyst was dispersed ultrasonically in 1 ml Nafion/ethanol (0.25 wt.% Nafion) for 30 min. Then 6 μl of the ink was pipetted and spread on the glassy carbon surface, and the electrode was air-dried. Cyclic voltammetry (CV) experiments were performed in 1.0 M KOH solution to obtain active area measurements, and in 1.0 M KOH + 1.0 M ethanol solution to measure the catalysts' activities towards ethanol anodic oxidation; the scan rate was 30 mV s^{-1} and the solutions were purged with N_2 for 20 min prior to each measurement.

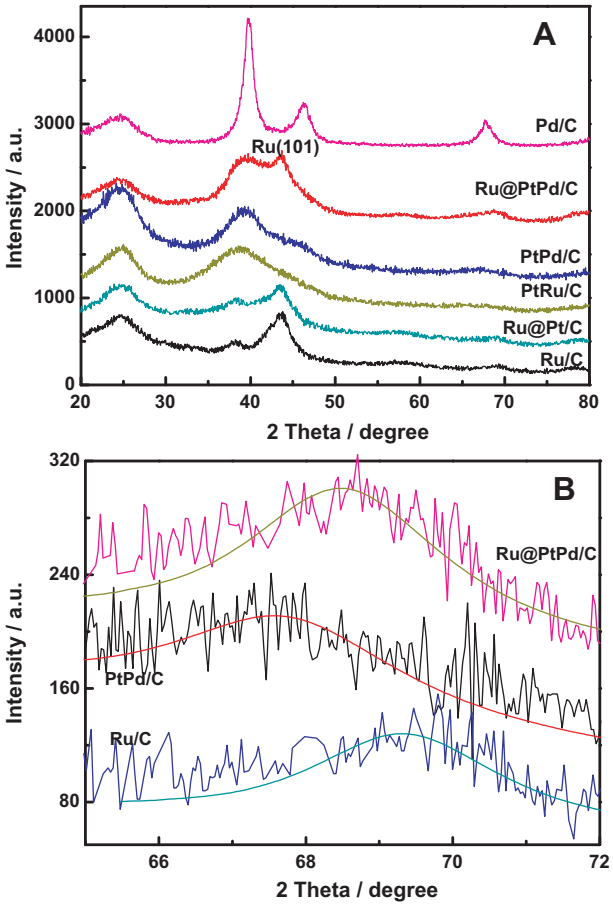

Fig. 1. X-ray diffraction patterns of Ru@PtPd/C, Ru@Pt/C, PtPd/C, PtRu/C, Pd/C, and Ru/C (A) and a detailed view of the peak profile for Ru@PtPd/C between 64° and 72° (B).

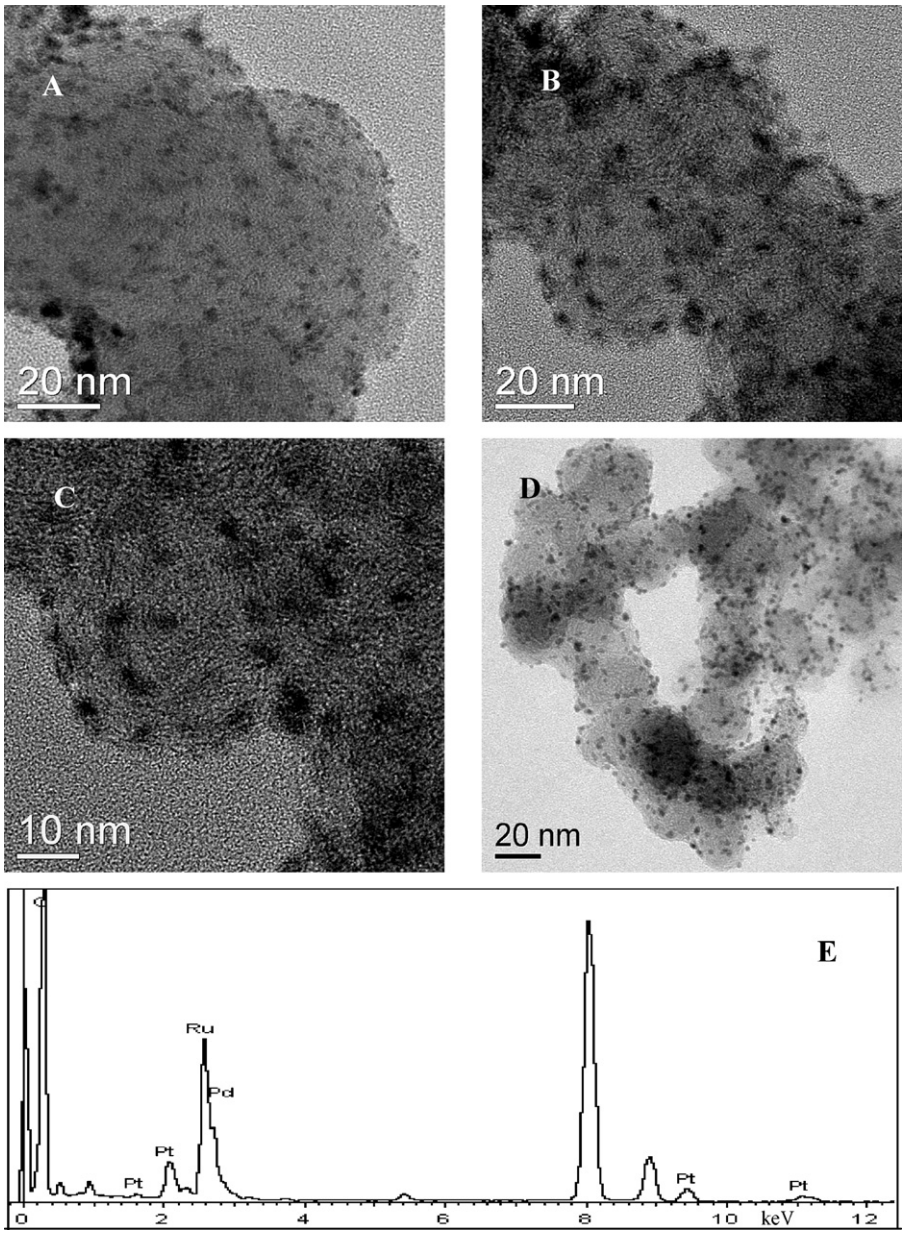

Fig. 2. TEM images of Ru/C (A), Ru@PtPd/C (B and C), and PtPd/C (D) catalysts, and the energy-dispersive X-ray analysis of Ru@PtPd/C (E).

3. Results and discussion

XRD is a bulk analysis tool that reveals a catalyst's crystal structure, lattice constants, and crystal orientation. The XRD patterns of the carbon-supported Ru@Pt and Ru@PtPd electrocatalysts are given in Fig. 1; those of the PtPd/C, PtRu/C, Pd/C, and Ru/C catalysts are also listed for comparison. The diffraction peak at $2\theta = 25^\circ$ is attributable to the carbon support. The reflection peaks for Ru/C at 38.4°, 44.0°, 58.3°, 69.3°, and 78.3° can be ascribed to Ru(1 0 0), Ru(1 0 1), Ru(1 0 2), Ru(1 1 0), and Ru(1 0 3), respectively. For Ru@Pt/C and Ru@PtPd/C, the diffraction peak of Ru(1 0 1) is apparently associated with diffraction peaks at ca. 39.0°, which are ascribed to Pt(1 1 1) and PtPd (1 1 1) [24], implying that Pt or PtPd was not alloyed with Ru. The main characteristic of XRD pattern for alloyed PtRu/C catalyst is that no diffraction peaks belong to ruthenium can be observed. It is reasonable to suggest that Pt or PtPd would be reduced and then cover the Ru particles. It can be assumed that (1) the interaction between the metals would be stronger than between metal and carbon [25] and (2) the creation of new nuclei is not energetically favorable in the solution phase [26]. The presence of a Ru(1 0 1) diffraction peak in Ru@Pt/C and Ru@PtPd/C may be due to the thin Pt and PtPd shell. It can be seen from the figure that the XRD patterns of Ru@Pt/C and Ru@PtPd/C are quite different from that of alloyed PtRu/C, in which the main diffraction peak is fcc (1 1 1) at ca. 39°, caused by the incorporation of ruthenium into the platinum lattice [27].

Fig. 1B shows a detailed view of the (2 2 0) diffraction. The catalysts' diffraction peaks have been fitted to Gaussian lines. The average size of the catalysts can be calculated using the Debye–Scherrer formula: $B_{2\theta} = 0.94\lambda/r\cos\theta$, where $B_{2\theta}$ is the width of a half peak, λ is the incident wavelength, r is the crystallite diameter, and θ is the diffraction angle. The average crystal sizes of Pd/C, PtPd/C, Ru/C, and Ru@PtPd/C catalysts are calculated to be ca. 5.0, 2.6, 2.5, and 2.9 nm, respectively. The particle size of Ru@PtPd/C is slightly bigger than that of Ru/C, which is possibly due to the PtPd alloy decorating the surface of the pre-formed Ru, the average thickness of the PtPd shell being around 0.2 nm. The particle size of PtPd/C is much smaller than that of Pd/C due to the addition of Pt to

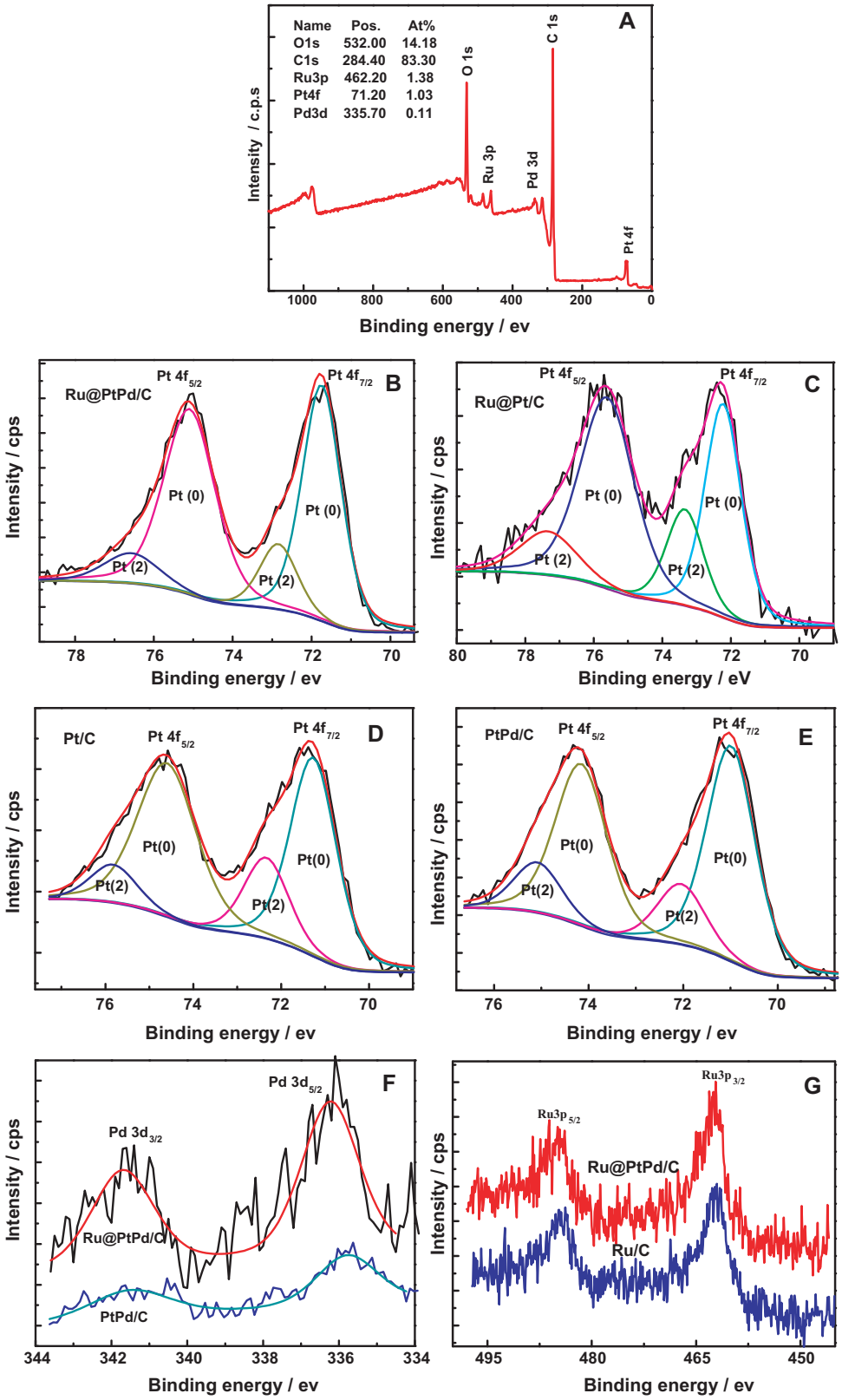

Fig. 3. XPS survey spectrum of Ru@PtPd/C (A); the Pt 4f core level XPS spectra of Ru@PtPd/C (B), Ru@Pt/C (C), Pt/C (D), and PtPd/C (E); Pd 3d (F); and the Ru 3p core level XPS spectra of the catalysts (G).

Pd. Also, the (2 2 0) diffraction of Ru@PtPd/C is located between the 2θ angles of pure Ru/C and alloyed PtPd/C, a phenomenon observed by other groups studying core-shell structured nanoparticles [25].

Fig. 2 shows TEM images of Ru/C (A) and Ru@PtPd/C (B and C). For comparison, PtPd/C sample prepared using the same procedure is also shown in Fig. 2D. In Fig. 2B the as-prepared Ru@PtPd/C catalyst shows a broader size distribution, centered on 3.1 nm, com-

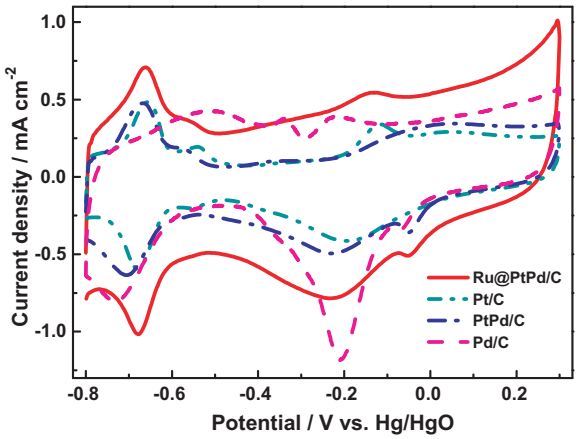

Fig. 4. Cyclic voltammograms of PtPd/C, Pd/C, Ru@PtPd/C, and Pt/C catalysts in nitrogen-saturated 1.0 M KOH solution (room temperature, scanning rate of 30 mV s^{-1}).

pared to that of Ru/C, which is centered on 2.7 nm. The average particle size for PtPd/C is 2.7 nm. These results are consistent with those obtained from the XRD data. Unfortunately, it is difficult to observe the core-shell structure using TEM. HRTEM images also failed to yield confirmed evidence for the core-shell structure of Ru@PtPd/C, but the slight increase in particle size may be a result of PtPd alloy covering the Ru core nanoparticles; in other words, it may be viewed as evidence of the core-shell structure of Ru@PtPd/C.

The composition of carbon-supported Ru@PtPd electrocatalyst was determined by energy-dispersive X-ray (EDX) analysis. The EDX composition of the prepared catalyst was found to be close to the nominal value.

XPS has been widely used to study the surface elemental composition and surface electronic structure of nanoparticles. The atomic ratio of Ru:Pt:Pd for Ru@PtPd/C is 1:0.75:0.08, which is higher than the nominal ratio of 1:0.3:0.06, indicating a PtPd-rich surface.

The Pt 4f spectra of the catalysts are shown in Fig. 3B–E. The Pt 4f signal in all the samples can be deconvoluted into two doublets. The peak position for Pt(0) at $4f_{7/2}$ is 71.2 and 72.4 eV for Pt/C, 71.0 and 72.2 eV for PtPd/C, 72.1 and 73.1 eV for Ru@Pt/C, and 71.8 and 72.8 eV for Ru@PtPd/C. The binding energies (BEs) of Pt in PtPd/C are negatively shifted compared with those of single Pt/C catalyst, and the same phenomenon occurs when comparing the BEs of Pt 4f in Ru@PtPd/C and Ru@Pt/C. The negative shift of Pt 4f peaks is possibly due to the addition of Pd and shows that electron transfer occurs from Pd to Pt (electronegativity: Pt = 2.28, Pd = 2.20). The Pt BEs of Ru@PtPd/C catalyst are higher than those of PtPd/C, indicating an interaction between the Ru core and the PtPd shell.

The Pd 3d levels of PtPd/C and Ru@PtPd/C in Fig. 3F show metallic palladium peaks only, with no peaks observable for palladium oxide. The metallic Pd $3d_{5/2}$ line for Ru@PtPd/C occurs at 336.2 eV, which is higher than that of PtPd/C (335.8 eV). The positive shift of Pd 3d and Pt 4f in the shell has been well understood by other groups [28].

The Ru 3p spectra in Fig. 3G are laden with noise and poorly resolved, making it difficult to quantify the BE states of Ru. However, the Ru in Ru@PtPd/C can still be clearly identified.

Fig. 4 displays the cyclic voltammograms of PtPd/C, Pd/C, Ru@PtPd/C, and Pt/C measured in N_2-purged 1.0 M KOH electrolyte at room temperature. The humps in the potential region −800 to −500 mV for Pt/C and −650 to −450 mV for Pd/C are associated with the hydrogen adsorption process in the anodic scan [29]. The electrochemical active surface area (ECSA) for the catalysts can be estimated from the integrated charge of the hydrogen adsorption region of the cyclic voltammograms [30]. The specific activity is

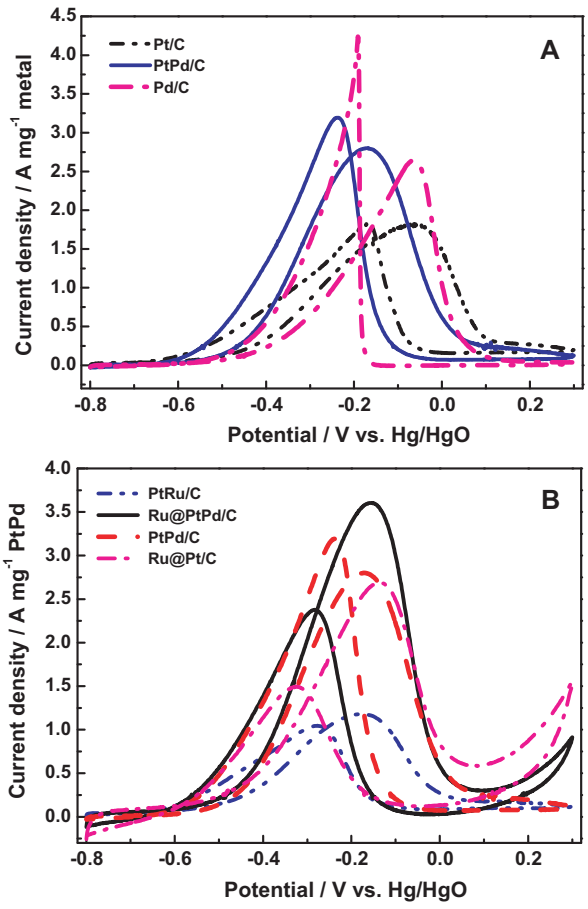

Fig. 5. Cyclic voltammograms of Pt/C, Pd/C and PtPd/C (A) and Ru@PtPd/C, Ru@Pt/C, PtRu/C and PtPd/C catalysts (B) in 1.0 M KOH solution + 1.0 M ethanol (room temperature, scanning rate of 30 mV s^{-1}).

calculated to be 42.0 $m^2 g^{-1}$ Pd for Pd/C, 32.2 $m^2 g^{-1}$ Pt for Pt/C, 80.3 $m^2 g^{-1}$ PtPd for Ru@PtPd/C, and 56.7 $m^2 g^{-1}$ PtPd for PtPd/C. The ECSA of PtPd/C is larger than that of Pd/C because of the former's smaller particle size, as evidenced by XRD. The ECSA of Ru@PtPd/C is 1.5 times as high as that of PtPd/C, which suggests higher utilization of Pt and Pd in Ru@PtPd/C.

The Ru@PtPd/C catalyst was evaluated for ethanol electrooxidation in 1.0 M KOH alkaline solution. The typical cyclic voltammograms of Pt/C, Pd/C, PtPd/C, Ru@PtPd/C, Ru@Pt/C, and PtRu/C for ethanol electrooxidation in 1.0 M KOH + 1.0 M ethanol solution at room temperature are presented in Fig. 5. Pd/C catalyst shows higher electrocatalytic activity toward ethanol oxidation than Pt/C, as shown in Fig. 5A, which is in agreement with other group's report [31]. The forward-sweeping peak current density of the PtPd/C catalyst for the EOR is almost the same as that of Pd/C, but the onset potential of the PtPd/C catalyst (−0.47 V) is 90 mV lower than that of the Pd/C catalyst (−0.38 V). The peak potential for the EOR on the PtPd/C catalyst is 100 mV more negative than that on the Pt/C and Pd/C catalysts, indicating the enhanced electrode kinetics, which may attributed to the better dispersion and smaller particle size.

Ru@PtPd/C shows superior catalytic activity to PtPd/C, PtRu/C and Ru@Pt/C – that is, lower onset potential and higher electrooxidation current density (Fig. 5B). The mass activity value of Ru@PtPd/C is 3.6 A mg^{-1} PtPd, which is about 2.0 times larger than Pt/C (1.8 A mg^{-1} Pt), 1.4 times larger than Pd/C (2.6 A mg^{-1} Pd) and 3.0 times larger than PtRu/C (1.2 A mg^{-1} Pt). The ethanol electrooxidation activity on Ru@PtPd/C is 1.3 times as high as that on PtPd/C, indicating enhanced electrocatalytic activity and rare metal uti-

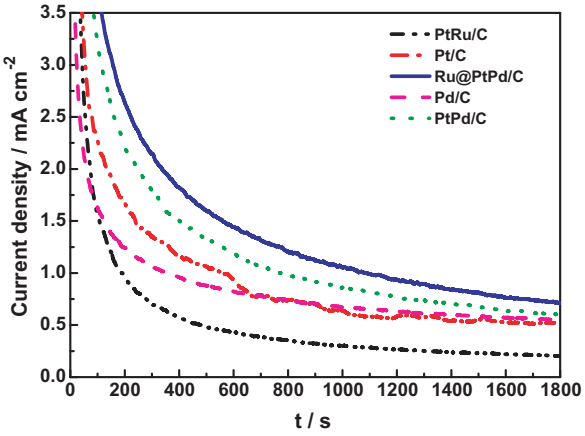

Fig. 6. Chronoamperograms of the catalysts at −0.4 V in 1.0 M ethanol + 1.0 M KOH at room temperature.

lization, which is caused by the better dispersion of PtPd and the higher ECSA. In addition, the higher activity on Ru@PtPd/C compared with Ru@Pt/C and on PtPd/C compared with Pt/C indicates the promoter action of Pd. It has been reported by other groups [32,33] that Pd shows high activity towards the ethanol oxidation reaction in alkaline media.

The ratio of forward peak current (I_f) to backward peak current (I_b) is generally used to characterize tolerance to CO-like oxidative intermediates generated during the oxidation of alcohol: a high ratio indicates more effective removal of the poisoning species from the catalyst surface. For Ru@PtPd/C, the I_f/I_b value was 1.5, which is 1.9 times higher than for PtPd/C (0.8), 2.5 times higher than for Pd/C, and 1.4 times higher than for the prepared PtRu/C catalyst (1.1), an indication of Ru@PtPd/C's greater poisoning tolerance to CO-like intermediates, due to its unique core-shell structure and enhanced PtPd utilization. The remarkably high mass-specific activity and good tolerance to CO_{ads} on Ru@PtPd/C indicates a more effective mechanism for promoting CO_{ads} removal, beyond the general "bifunctional mechanism".

Fig. 6 shows the chronoamperometric curves of the catalysts in 1.0 M ethanol + 1.0 M KOH at −0.4 V. The potential of the working electrode with Pt/C, Pd/C, PtPd/C, PtRu/C, and Ru@PtPd/C was fixed at −0.4 V and the changes in the electrooxidation current with time were recorded. For all of the catalysts, the current decayed continuously during the evaluation period, supposedly because of catalyst poisoning by the chemisorbed carbonaceous species. The quasi-stable current densities of Pt/C, Pd/C, PtPd/C, PtRu/C, and Ru@PtPd/C at 1800 s were 0.50, 0.55, 0.62, 0.20, and 0.73 mA cm^{-2}, respectively. Ru@PtPd/C presented a higher current density at end of the test compared to Pt/C, Pd/C, PtRu/C, and PtPd/C catalysts, indicating the higher stability of Ru@PtPd/C than those of the other four catalysts.

4. Conclusions

The anodic oxidation of ethanol on a core-shell structured Ru@PtPd/C catalyst, prepared by deposition of PtPd on a pre-formed Ru/C catalyst, has been investigated in alkaline media. Significantly enhanced activity and stability have been achieved using this core-shell catalyst. Ru@PtPd/C was characterized using XRD, TEM, and XPS, and the results supported the existence of a core-shell structure.

Acknowledgments

We would like to thank the National Scientific Foundation of China (NSFC Project nos. 20673040 and 20876062), the Ministry of Science and Technology of China (no. 2009AA05Z119), and the Fundamental Research Funds for the Central Universities of South China University of Technology for financial support of this work.

References

[1] A. Hamnett, Catal. Today 38 (1997) 445–457.
[2] X. Ren, P. Zelenay, S. Thomas, J. Davey, S. Gottesfeld, J. Power Sources 86 (2000) 111–116.
[3] B. Gurau, E.S. Smotkin, J. Power Sources 112 (2002) 339–352.
[4] F. Vigier, C. Coutanceau, F. Hahn, E.M. Belgsir, C. Lamy, J. Electroanal. Chem. 563 (2004) 81–89.
[5] E. Antolini, J. Power Sources 170 (2007) 1–12.
[6] S. Sen Gupta, J. Datta, J. Electroanal. Chem. 594 (2006) 65–72.
[7] M. López-Atalaya, E. Morallón, F. Cases, J.L. Vázquez, J.M. Pérez, J. Power Sources 52 (1994) 109–117.
[8] S.C.S. Lai, M.T.M. Koper, Phys. Chem. Chem. Phys. 11 (2009) 10446–10456.
[9] W.J. Zhou, S.Q. Song, W.Z. Li, Z.H. Zhou, G.Q. Sun, Q. Xin, S. Douvartzides, P. Tsiakaras, J. Power Sources 140 (2005) 50–58.
[10] J.W. Gosselink, Int. J. Hydrogen Energy 27 (2002) 1125–1129.
[11] G.A. Camara, R.B. de Lima, T. Iwasita, Electrochem. Commun. 6 (2004) 812–815.
[12] S.C.S. Lai, S.E.F. Kleyn, V. Rosca, M.T.M. Koper, J. Phys. Chem. C 112 (2008) 19080–19087.
[13] J. Shin, W.J. Tornquist, C. Korzeniewski, C.S. Hoaglund, Surf. Sci. 364 (1996) 122–130.
[14] U. Schmiemann, U. Müller, H. Baltruschat, Electrochim. Acta 40 (1995) 99–107.
[15] F. Colmati, E. Antolini, E.R. Gonzalez, J. Power Sources 157 (2006) 98–103.
[16] J.F. Gomes, B. Busson, A. Tadjeddine, J. Phys. Chem. B 110 (2006) 5508–5514.
[17] W.J. Zhou, W.Z. Li, S.Q. Song, Z.H. Zhou, L.H. Jiang, G.Q. Sun, Q. Xin, K. Poulianitis, S. Kontou, P. Tsiakaras, J. Power Sources 131 (2004) 217–223.
[18] M.H. Huang, L.R. Li, Y.L. Guo, J. Solid State Electrochem. 13 (2009) 1403–1409.
[19] J. Datta, S. Singh, S. Das, N.R. Bandyopadhyay, Bull. Mater. Sci. 32 (2009) 643–652.
[20] H.Q. Li, G.Q. Sun, L. Cao, L.H. Jiang, Q. Xin, Electrochim. Acta 52 (2007) 6622–6629.
[21] E.V. Spinacé, A.O. Neto, T.R.R. Vasconcelos, M. Linardi, J. Power Sources 137 (2004) 17–23.
[22] Z. Bai, L. Yang, L. Li, J. Lv, K. Wang, J. Zhang, J. Phys. Chem. C 113 (2009) 10568–10573.
[23] H. Gao, S. Liao, J. Zeng, Y. Xie, J. Power Sources 196 (2011) 54–61.
[24] T. Lopes, E. Antolini, E.R. Gonzalez, Int. J. Hydrogen Energy 33 (2008) 5563–5570.
[25] R. Wang, H. Li, H. Feng, H. Wang, Z. Lei, J. Power Sources 195 (2010) 1099–1102.
[26] J. Zeng, J.Y. Lee, W. Zhou, J. Power Sources 159 (2006) 509–513.
[27] J.T. Moore, J.D. Corn, D. Chu, R. Jiang, D.L. Boxall, E.A. Kenik, C.M. Lukehart, Chem. Mater. 15 (2003) 3320–3325.
[28] Y.N. Wu, S.J. Liao, Y.L. Su, J.H. Zeng, D. Dang, J. Power Sources 195 (2010) 6459–6462.
[29] R. Pattabiraman, Appl. Catal. A 153 (1997) 9–20.
[30] W. Li, P. Haldar, Electrochem. Commun. 11 (2009) 1195–1198.
[31] C.P. Xu, K. Shen, Y. Liu, J. Power Sources 164 (2007) 527–531.
[32] F. Hu, G. Cui, Z. Wei, P.K. Shen, Electrochem. Commun. 10 (2008) 1303–1306.
[33] Z.X. Liang, T.S. Zhao, J.B. Xu, L.D. Zhu, Electrochim. Acta 54 (2009) 2203–2208.